ACCSCIENCE PUBLISHING

Materials Science in Additive Manufacturing

ORIGINAL RESEARCH ARTICLE

Selective laser melting of ferritic/martensitic oxide dispersion-strengthened steel: Processing, microstructure, and mechanical properties

Maria Zaitceva*, Artem Borisov, Anatoliy Popovich, and Vadim Sufiiarov

Institute of Machinery, Materials and Transport, Peter the Great St. Petersburg Polytechnic University, Saint Petersburg, Russia

Abstract

Oxide dispersion-strengthened (ODS) ferritic/martensitic steels have emerged as a promising structural material for nuclear power applications due to their high heat resistance. However, the fabrication of complex ODS steel components remains a significant challenge. T his study presents the influence of the main selective laser melting process parameters and heat treatment on the densification, microstructure, and tensile properties at room and elevated temperatures of high chromium ferritic/martensitic ODS steel strengthened with 0.25 wt.% yttrium oxide (Y_2O_3). The optimization of process parameters and platform pre-heating enabled the production of parts with a density above 98%. The application of pre-heating allowed for higher scanning speeds to be used to achieve similar relative density and avoid cracking. Partial recrystallization after heat treatment was noted, affecting grain morphology by increasing equiaxedness and decreasing size. X-ray analysis was employed to determine the phase composition. However, the results were ambivalent and required confirmation by other methods. The addition of 0.25 wt.% Y_2O_3 resulted in an ultimate tensile strength value of 978 MPa for the as-built material at room temperature. At elevated temperatures, the properties are comparable to those of the base steel, indicating the necessity for further research.

Keywords: Selective laser melting; Oxide dispersion-strengthened steel; Tensile testing; Heat treatment; Additive manufacturing; ODS steel; Laser powder bed fusion

***Corresponding author:**
Maria Zaitceva
(zajtsevamya@yandex.ru)

Citation: Zaitceva M, Borisov A, Popovich A, Sufiiarov V. Selective laser melting of ferritic/martensitic oxide dispersion-strengthened steel: Processing, microstructure and mechanical properties. *Mater Sci Add Manuf.* 2025;4(1):025060004. doi: 10.36922/MSAM025060004

Received: February 6, 2025

1st revised: February 28, 2025

2nd revised: March 11, 2025

Accepted: March 12, 2025

Published online: March 24, 2025

1. Introduction

Ferritic/martensitic oxide dispersion-strengthened (ODS) steels are regarded as promising candidates for structural materials in next-generation nuclear reactors. This is attributed to their high radiation resistance and acceptable mechanical properties at elevated temperatures.[1] The desirable properties of ODS steels result from the presence of stable nanosized oxide particles, which inhibit grain boundary and dislocation migration, thereby maintaining the material's microstructural stability during service. In addition, the interfaces between matrix and dispersed oxides can serve as sinks for radiation-induced defects, which result in increasing irradiation resistance.[2] ODS steels based on high chromium ferritic/martensitic steels containing 9 – 12 wt.% Cr have garnered significant interest due to their proven performance in past fast reactors. Furthermore, ferritic/martensitic steels are highly resistant to void

swelling,[3] which is quite necessary for nuclear reactor application.

At present, the most extensively studied and widely utilized method of strengthening involves the incorporation of yttrium-based nano-oxides. Numerous studies have demonstrated the efficacy of yttrium oxide (Y_2O_3) additions in enhancing the mechanical strength of steels and various other alloys. This enhancement in strength is accompanied by an improvement in resistance to radiation-induced swelling under exposure to fission ions or neutrons. Furthermore, dispersion strengthening through nano-oxides significantly increases the hardness of the matrix material, thereby contributing to an improvement in wear resistance.[4] The most common addition of oxides is in the order of 0.25 – 1.0 wt.%. In addition to yttrium, other elements may be added to form complex oxides such as $Y_nX_mO_p$, where X = Ti, Al, Zr, Hf, V, Si, or Ta.[5,6] The formation enthalpy of this type of oxide is lower than that of Y_2O_3.

The fabrication of ODS steels remains a significant challenge. The most prevalent method of production involves powder metallurgy, specifically mechanical alloying.[7-10] Creating products with complex geometries using powder metallurgy methods is an expensive and time-consuming process. One of the most common processes used to produce ODS steels is hot isostatic pressing (HIP)[2,11,12] and spark plasma sintering.[13-15] However, the use of these techniques is advisable in cases of production of simple and symmetrical shapes.

Another critical limitation is the relatively poor weldability of ODS steels, which increases the cost and complexity of manufacturing components with intricate geometries. Consequently, there is growing interest in exploring the feasibility of producing ODS steels through additive manufacturing (AM) techniques. AM has already shown itself to be a state-of-the-art manufacturing process that allows the production of complex-shaped products with high mechanical properties. One of the most commonly used technologies for the production of metal products is selective laser melting (SLM). The process consists of layer-by-layer laser processing of powder material according to a CAD model. SLM technology is already widely used in areas such as aerospace, medicine, and turbine engineering. An important feature of the SLM process is the high cooling rates (10^3 – 10^8 K/s).[16]

A number of published studies demonstrate the feasibility of producing ODS steels by SLM.[1,5] A study suggests that optimization of the process parameters could lead to a density of more than 98%.[17] The results also showed the possibility of obtaining a material with a uniform distribution of nanosized oxides. However, the size of oxides in the materials obtained by SLM is larger (in the order of 30 – 60 nm), compared to particles obtained by powder metallurgy methods (typically 1 – 10 nm).[18-20] The size of the yttrium-based dispersoids influences coherency, and the size above 20 nm results in agglomeration and coarsening,[21] which reduces the positive effect of their implementation.

A notable challenge associated with the use of powders derived from mechanical alloying is their splintered morphology,[22] resulting from the high mechanical stresses applied during the process. This irregular particle shape leads to poor flowability, which may be a limitation for the applications of mechanically alloyed powders in AM.[23] Furthermore, studies have demonstrated that the morphology and particle size distribution of the powder material significantly influences the final properties of products fabricated through AM methods. To address these limitations, mechanically alloyed powders require spheroidization before use.[24] The plasma spheroidization process involves a melting stage during which oxide particles tend to coagulate and migrate to the surface of the molten material due to their relatively lower density compared to the metallic matrix. Consequently, the resulting spherical powder exhibits non-uniform oxide dispersion,[24] which can negatively impact the mechanical properties of the final product.

For the production of ODS steels by SLM, not only can mechanically alloyed powders be used, but also various *in situ* synthesis methods when oxides are forming during the printing process. In Jia *et al.*'s study,[25] pre-alloyed powders were used for the *in situ* synthesis of nanoparticles in ODS steel during SLM by controlling the partial pressure of oxygen to prevent the abnormal growth of particles. This approach resulted in the formation of a microstructure characterized by finer nanoparticles, a higher volume fraction, and a more uniform spatial distribution and size consistency compared to the majority of ODS steels manufactured using SLM with mechanically alloyed powders. The influence of the properties of *in situ* formed nitride and oxide particles in the ODS steel produced by laser powder bed fusion in a nitrogen-rich atmosphere (with Y_2O_3 = 0.45 wt.%) was studied by Cakmak *et al.*[26] The incorporation of nanosized Y_2O_3 reduces the length of typical for SLM as-built parts columnar grains (from 70 μm to 40 μm).[26] In addition to Y_2O_3, Al-O aluminum oxides, and Y-Al-O yttrium aluminum oxides were observed in the microstructure. A significant challenge in the production of ODS steel through *in situ* synthesis during the SLM process lies in the inherent complexity of the technological workflow. This complexity necessitates precise monitoring and control of all process parameters

to ensure the consistency and stability of the material's quality.

In addition to mechanical alloying, soft-mixing techniques are employed to produce ODS steels by SLM.[27] This approach facilitates uniform adhesion of oxide particles onto the surface of steel powders, in contrast to alloying processes involving dispersed particles of the matrix material. By maintaining the original spherical morphology of the powder particles, the soft-mixing method ensures good flowability. The advantage of this method of powder preparation is the relatively simple and fast mixing process compared with mechanical alloying. Zhai *et al.*[28] investigated the influence of interface wettability of 316L ODS steel strengthened by Y_2O_3 on tensile properties. Poor interface wettability of the nanoparticles and the basic steel was the reason for the Y_2O_3 agglomerations forming, which led to internal defects. Besides, the increases in yield strength (YS) and ultimate tensile strength (UTS) were neglectable, and the nanoparticle agglomeration significantly decreased the elongation. The results of the investigation and comparison of tensile properties and tribological behavior of the two alloys (basic and ODS) fabricated by SLM showed a significant reduction in wear rate (by 51%) when 0.3 wt.% Y_2O_3 nanoparticles were added compared to the matrix alloy.[1]

The acoustic mixing method has been successfully utilized to achieve a uniform distribution of oxides in a NiCoCr medium-entropy alloy.[23] The introduction of 1 wt.% Y_2O_3 led to a significant enhancement in mechanical properties, as confirmed by tensile testing. Notably, the addition of Y_2O_3 resulted in a marked improvement in strength, particularly at elevated temperatures, highlighting the efficacy of this approach in optimizing high-temperature performance.

Presently, the details of AM processes of high chromium ferritic/martensitic steels remain underexplored. These steels are susceptible to cracking, which complicates their production by methods such as SLM. There are virtually no studies devoted to the investigation of the production of ODS steels based on high-chromium ferritic/martensitic steels, despite their promising application in nuclear power engineering.

This research is aimed at studying the possibilities of fabrication of ferritic/martensitic ODS steel by SLM and analyzing the structure and tensile properties of the obtained material, including at elevated temperatures (720°C). The present study also employed platform pre-heating as a method to mitigate cracking and enhance material density. Given the significance of this steel in the context of next-generation reactor applications, the tensile properties were assessed within the anticipated operational temperature range. This study will serve as a basis for subsequent studies aimed at studying the specifics of the production of high chromium ferritic-martensitic ODS steels.

2. Materials and methods

2.1. Materials

In this study, ferritic-martensitic steel powder with the chemical composition presented in Table 1 was employed as the base material. The base gas atomized ferritic/martensitic steel powder had a particle size distribution of 22 – 63 μm.

For the production of ODS steel through SLM, the base steel powder was mixed with 0.25 wt.% Y_2O_3 using an acoustic mixing process. The acoustic mixing process was performed on a laboratory unit. The particle size distribution study was carried out on an Analysette 22 NanoTec plus analyzer (Fritsch GmbH, Idar-Oberstein, Germany) operating in the particle measurement range from 0.01 to 2000 μm. The flowability of the powder was determined using a Hall flowmeter.

2.2. SLM and heat treatment

The SLM process was performed on a 3DLAM Mid system (Biograd CJSC, St. Petersburg, Russia) equipped with a platform pre-heating module capable of achieving temperatures up to 300°C and a laser with a maximum output power of 500 W. To optimize the process parameters, two sets of samples were fabricated: One without the platform pre-heating and another with the platform pre-heating of 300°C. Each set comprised 20 cubic samples (10 mm × 10 mm × 10 mm) produced directly on the baseplate without supporting structures. Scanning speed and laser power were systematically varied, while the hatching distance was maintained at 120 μm, and the layer thickness was fixed at 30 μm. The applied SLM process parameters are detailed in Table 2. A stripe-hatching pattern with a 67° rotation between layers was employed to enhance mechanical properties and minimize residual stresses.[29]

Since the energy input to the material significantly affects melt pool formation and the properties of the resulting structure, the volumetric energy density (*VED*, J/mm^3) was calculated using the following equation:

$$VED = P/(v \times h \times t), \quad \text{(I)}$$

where P = laser power (W); v = scanning speed (mm/s); h = hatch distance (mm); and t = layer thickness (mm).

The typical heat treatment mode for this material involves quenching at 1050 – 1100°C for 30 min, followed

Table 1. Chemical composition of the base ferritic/ martensitic steel

Element	C	Si	Mn	Cr	Ni	Mo	Nb	V	P	Fe
wt. %	0.12	0.2	0.2	12.1	0.1	1.3	0.35	0.2	0.001	Bal.

Table 2. Process parameters of selective laser melting

Parameters	Range
Laser power	150 – 225 W
Scanning speed	420 – 820 mm/s
Hatch distance	120 μm
Layer thickness	30 μm

by high-temperature annealing at 720°C for 60 – 180 min.[30] In the present study, the heat treatment was performed in a vacuum at 1050°C for 30 min with subsequent quenching, followed by high-temperature annealing at 720°C for 60 min. The heat treatment process was carried out using a vacuum furnace Carbolite Gero LHTW 200 – 300/22-1G (Carbolite Gero Ltd., Derbyshire, UK).

2.3. Characterization

Subsequent to the printing process, the samples were separated from the platform by wire-cut electrical discharge machining. The estimation of the density of all samples was performed by the Archimedes method. Cubic samples with dimensions of 10 mm × 10 mm × 10 mm were prepared for microstructural investigations, phase composition analysis, and microhardness testing. The samples were pressed into epoxy resin and then subjected to grinding and mechanical polishing. Porosity and inner defects fraction were calculated of the pore fraction in relation to the whole image plane using ImageJ image analysis software on optical microscope images with ×50 magnification. The grain size estimation was performed using optical micrographs along the building direction.

Phase analysis was conducted using a Bruker D8 Advance X-ray diffractometer (XRD; Bruker Corporation, Billerica, MA, USA) with Cu-Kα radiation (a = 1.5418 Å) in the range 2θ = 30° – 100°. A scanning interval of 0.02° was used. Before microstructural analysis, the specimens were etched using a 3:1 solution of hydrochloric acid and nitric acid. The microstructural characterization was carried out utilizing a Leica DMI5000 optical microscope (Leica Microsystems GmbH, Wetzlar, Germany) and a Tescan Mira3 LMU scanning electron microscope (SEM) (TESCAN GROUP, Brno, Czech Republic).

The hardness of the samples was evaluated using a Buehler Micromet 5103 hardness tester (Buehler Ltd., USA) employing the Vickers hardness method. The tests were carried out at a load of 10 N with a dwell time of 5 s. Uniaxial tensile tests were performed on three specimens for each condition to determine the tensile strength, YS, and relative elongation of the specimens. The specimens' blank parts were initially printed, heat-treated, and then machined. These tests were performed under ambient conditions using a Zwick/Roell z100 tensile testing machine. Tensile testing at an elevated temperature of 720 ± 10°C was carried out using a Zwick/Roell z050 machine (ZwickRoell GmbH & Co., Ulm, Germany). For all the specimens, tests were carried out under a crosshead displacement velocity of 0.8 mm/min on the elastic section, and 2 mm/min on the plastic section. An examination of the fractured surfaces from the tensile tests was conducted using SEM.

3. Results and discussion

3.1. Material preparation

The application of acoustic mixing facilitated the production of steel powder with a spherical morphology and uniformly distributed oxide particles on the surface, as demonstrated by the SEM image (Figure 1). The presence of nanosized oxides on the particle surfaces resulted in a slight reduction in the powder's flowability, from 12 s/50 g to 16 s/50 g. Zhai *et al.*[28] reported the flowability of ODS 316L-Y_2O_3 steel powder was not decreased after low-energy ball milling. Nevertheless, the outcome can be ascribed to the diminished wettability and flowability of Y_2O_3, which, being located on the surface of the base material particles, predictably reduces the flowability of the obtained material. However, flowability remains for utilization in the SLM process.

3.2. The influence of SLM process parameters on relative density

The effects of laser power and scanning speed on relative density are presented in Figure 2. Laser power varied in the range from 150 to 225 W. As the laser power increases, the relative density increases until it reaches a threshold value of VED. In general, the density of samples fabricated using laser powers of 200 W and 225 W is higher compared to those produced with laser powers of 150 W and 175 W. Scanning speed varied in the range from 420 to 820 mm/s. Contrary to the influence of laser power, increasing scanning speed resulted in lower density. A similar tendency has been observed in another study.[31]

When samples were fabricated without platform pre-heating, all of them exhibited horizontal surface cracks, caused by thermal stresses arising from high temperature gradients during the SLM process. To address this issue, a set of samples was fabricated using a platform pre-heating

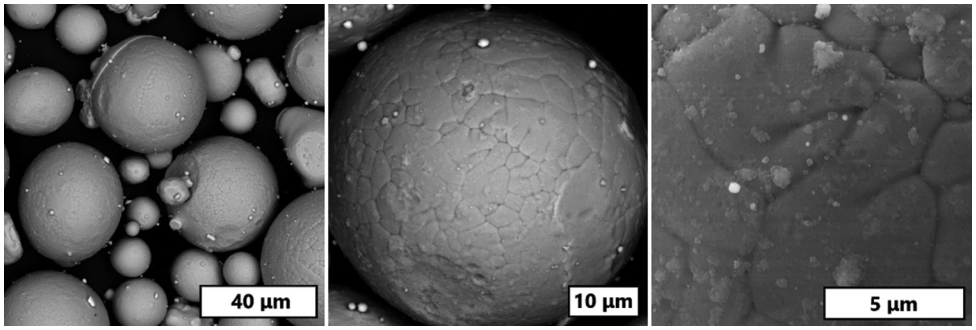

Figure 1. SEM-BSE images of the mixed ODS-steel powder. Magnification: 2000×, 5000×, 20000×
Abbreviations: BSE: Backscattered electrons; SEM: Scanning electron microscopy.

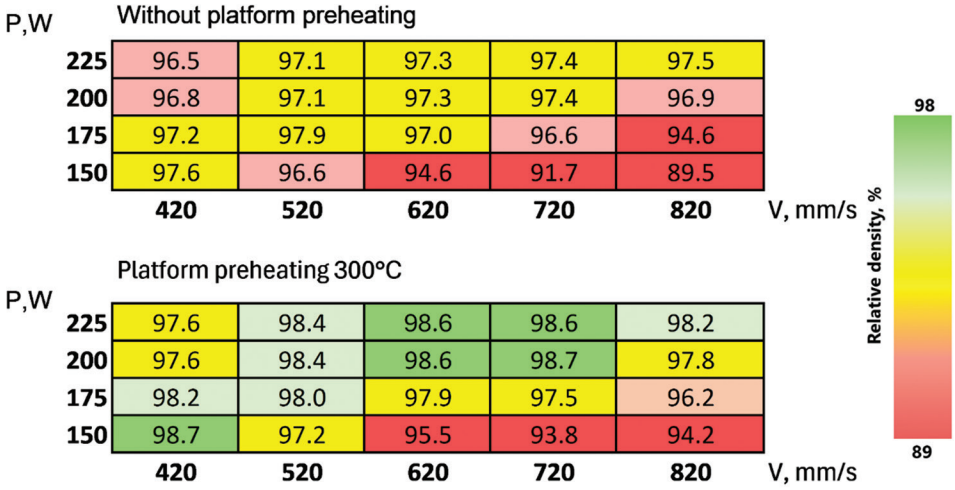

Figure 2. Effect of laser power (*P*) and scanning speed (*V*) on the density of as-built SLM material
Abbreviation: SLM: Selective laser melting

at 300°C to reduce the temperature gradient during printing.

In Figure 3, the effect of *VED* of the SLM process on relative density is shown. When pre-heating was applied, the trends of influence of laser power and scanning speed on the density of as-built SLM material were the same as it was observed without pre-heating. However, density depending on these parameters, did not exhibit very pronounced variations. The lowest density was obtained with the *VED* lower than 70 J/mm^3. It can be attributed to a lack-of-fusion defect formation. This type of defect can be seen in Figure 4, which resulted in a significant reduction in material density. Conversely, samples produced at high energy densities (higher than 110 J/mm^3) exhibited spherical pores as a result of changing melting from conduction to key-hole mode and attributed to material overheating.

Platform pre-heating not only resolved the surface cracking issue but also enhanced the material density,

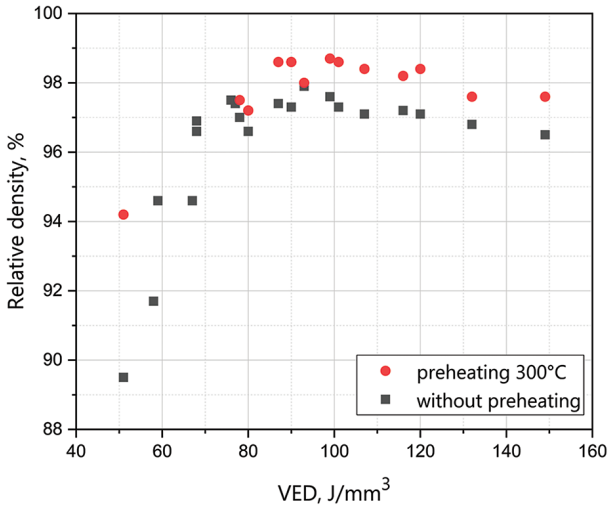

Figure 3. Effect of VED on the relative density of as-built SLM material with and without platform pre-heating
Abbreviations: SLM: Selective laser melting; VED: Volumetric energy density

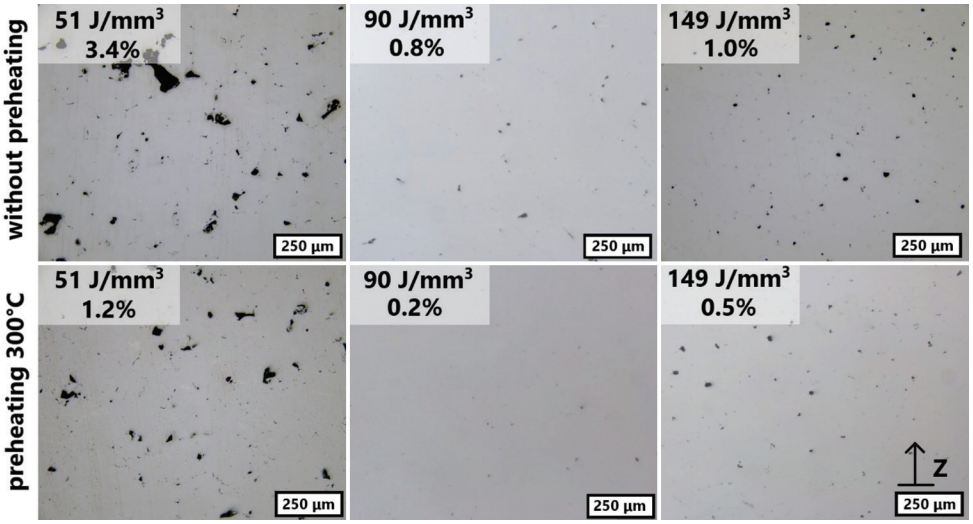

Figure 4. Macrostructure of the as-built SLM samples. VED and porosity values of the samples are presented. Magnification: ×100
Abbreviations: SLM: Selective laser melting; VED: Volumetric energy density

as evidenced by the density measurements presented in Figure 3 and the microstructural observations in Figure 4. It was demonstrated that when the same SLM process parameters with pre-heating are employed, the relative density is increased. This, in turn, facilitates the use of higher scanning speeds to achieve equal density. This finding is also consistent with the results obtained by Qin *et al.*[32] The range of *VED* from 80 to 110 J/mm³, and pre-heating allow for building samples with a density above 98%. Numerous studies have shown[33] that the application of HIP results in decreasing porosity of AM parts, thereby enhancing their mechanical properties.[34] This process is planned to be studied in future research.

The obtained specimens exhibit no visible defects, such as cracks or lack-of-fusion. While the highest material density was obtained at *VED* values in a range of 90 – 100 J/mm³, all samples printed within this energy range exhibited discontinuities between the contours and the bulk material. In addition, their surface quality was inferior compared to samples fabricated at higher *VED* values. To align both density and surface quality, a hybrid approach was implemented wherein the contours were built with the higher *VED*, and for the bulk material fabrication, *VED* of 90 J/mm³ was applied. This method resulted in improved material density by minimizing internal defects and enhanced surface quality. All subsequent analyses were conducted on samples fabricated using this optimized mode.

3.3. Microstructural characterization

The X-ray diffraction (XRD) analysis revealed that all samples exhibited the same phase composition,

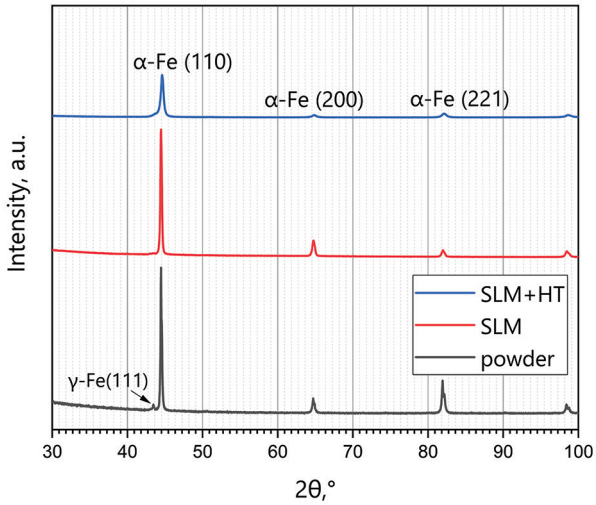

Figure 5. X-ray diffraction lines of mixed powder and fabricated specimens
Abbreviations: HT: Heat treatment; SLM: Selective laser melting

characterized by peaks corresponding to the body-centered cubic lattice of iron, as shown in Figure 5. No carbide phases were detected on the XRD, likely due to the low volume fraction and nanoscale size (up to 300 nm) of carbide particles. Apparently, the mass fraction and size of precipitates are lower than the XRD analysis method allows to determine.[35,36] Similarly, determining Y_2O_3 peaks is also challenging.

After heat treatment, a displacement of the peaks slightly toward higher 2θ angles was observed. This phenomenon may be explained by the removal of internal stresses. The peak corresponding to the position of the

face-centered cubic iron phase peak (2θ = 43.1°) in the powder probably indicates the presence of a small amount of residual austenite. However, after SLM, this peak intensity undergoes a notable reduction. This is probably due to the lower cooling rates of SLM compared to gas atomization. This observation signifies a modification in the material's structural configuration, probably related to the redistribution of chromium and carbon in the process. The evident broadening of the peaks of the material after heat treatment signifies a reduction in grain size, which was further supported by the microstructural observations presented in Figure 6.

The microstructure of the samples after SLM with pre-heating is characterized by columnar grains oriented along the building direction, as shown in Figure 6A and B, which are typical for this group of materials in SLM production.[17] The appearance of melt pools and heat-affected zones, typically observed after SLM, is not strongly evident in our samples.[37] However, the addition of Y_2O_3 decreased the grain length compared to the base material.[38] The base steel produced by SLM without pre-heating exhibited an average grain length of 156 μm and an average grain width of 30 μm.[38] After the incorporation of 0.25 wt.% Y_2O_3, the average grain length decreased to 112.0 ± 20 μm, and the average grain width increased to 57.0 ± 11 μm. In a previous study, Ghayoor *et al.*[39] reported a significant change in grain shape from columnar to equiaxed when 5 wt.% yttrium was added to 304 L steel. A decrease in grain length has also been observed in other research.[26] The application of platform pre-heating results in a decrease in the temperature gradient, consequently leading to the creation of more favorable conditions for epitaxial growth during the transition between layers and the formation of elongated grains along the building direction. The sample obtained by SLM with pre-heating is characterized by an average grain length of 133.2 ± 55 μm and an average width of 21.1 ± 8 μm. After heat treatment, the material became partially recrystallized and the shape of the grains was almost equiaxed. The grain size reduction in heat-treated samples, as compared to materials before heat treatment, is shown in Figure 7. The average grain length and width decreased to 39.9 ± 11 μm and 18.5 ± 7 μm, respectively. The structure obtained after heat treatment became more similar to the structure of materials fabricated by conventional manufacturing methods.[36] Besides, the formation of small equiaxed grains was also observed. Y_2O_3 probably act as crystallizing centers during heterogeneous nucleation, resulting in smaller equiaxed grains.

3.4. Mechanical properties

Finally, the tensile properties of the samples produced by SLM with and without subsequent heat treatment were assessed. The results of tensile testing at room and at

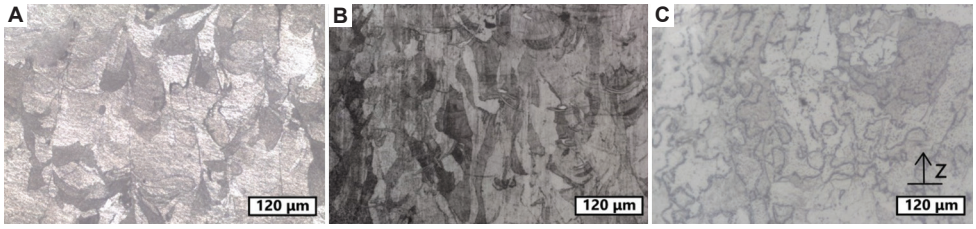

Figure 6. Microstructure of samples: (A) SLM sample without pre-heating, (B) SLM sample pre-heating at 300°C, and (C) SLM sample after heat treatment. ×200
Abbreviation: SLM: Selective laser melting

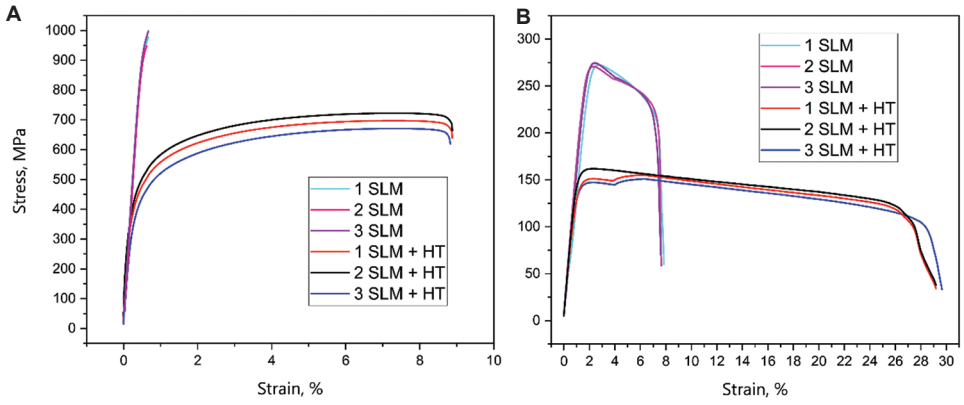

Figure 7. Stress strain curves for samples after SLM without and with heat treatment tested at: 20°C (A) and 720°C (B).
Abbreviations: HT: Heat treatment; SLM: Selective laser melting

operating (720°C) temperatures are presented in Figure 7 and Table 3. The results of the tests conducted on specimens produced without pre-heating are not presented. This decision is due to the presence of a significant number of cracks in the specimens, which made the tests invalid.

The as-built SLM ODS specimens exhibited a brittle behavior. At room temperature, fracture occurred at 978 MPa with no evidence of plastic deformation before fracture. This UTS value was comparable to the values for the similar ferritic/martensitic ODS steel plates and tubes manufactured through powder metallurgy (UTS = 991 MPa),[40] but the problem was YS and elongation was absent. Following heat treatment, the mechanical response of the SLM ODS specimens during tensile transition to a ductile mode. The YS and UTS achieved were lower than the base steel produced through powder metallurgy techniques (YS = 525 MPa, UTS = 711 MPa, ε = 16%).[41] The elongation of the heat-treated SLM ODS specimens remained significantly lower than that of the powder metallurgy-derived base material. The findings revealed the substantial impact of incorporating 0.25 wt.% Y_2O_3 on the tensile properties. In a prior investigation of base steel produced by SLM, the maximum tensile strength was also observed for the specimen after SLM without heat treatment. The UTS was 567 MPa, aligning with the absence of plastic characteristics.[38] Consequently, the incorporation of Y_2O_3 resulted in a 72% increase in UTS compared to the base steel.

The mechanical properties of heat-treated SLM samples, when tested at elevated temperatures, were not very significant. The tensile properties of the material tested at 720°C after SLM were comparable to those of base steel obtained by powder metallurgy methods (YS = 279 MPa, UTS = 284 MPa, ε = 25%).[41] However, the elongation was much lower. The relatively low ductility of all specimens after SLM can be explained by the quenched state and internal stresses.

Fractography was used to study the fracture surfaces of the specimens. From Figure 8, it can be observed that the SLM specimen tested at 20°C exhibited an undeveloped fracture surface. The fracture occurred without necking, and the fracture mode appears to be of an intergranular nature. The specimen, after heat treatment, featured a more developed fracture surface with a few cleavage platforms and a number of dimples. As the specimen after SLM underwent tensile testing at 720°C, its fracture surface exhibited a significant increment in the number of dimples of a lower size. The fracture character of the specimens is classified as higher ductility, accompanied by the presence of brittle fracture areas. The specimen after SLM and heat treatment tested at 720°C had dimples and micro-voids, an indication of the ductile nature of the fracture. In all the cases, no visible cracks, inclusions, or unmelted powder particles were detected.

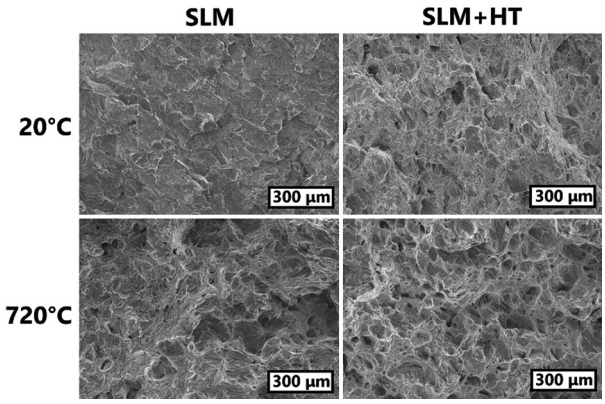

Figure 8. Fracture surfaces of samples after SLM without and with heat treatment after tensile testing at 20°C and 720°C. Magnification: ×100
Abbreviation: SLM: Selective laser melting

Table 3. Tensile properties of specimens fabricated in the present work

Condition	Temperature, °C	YS, MPa	UTS, MPa	ε, %
SLM ODS	20	-	978±24	-
	720	266±2	272±2	7.7±0.1
SLM ODS+HT	20	440±14	697±25	8.6±0.2
	720	144±8	156±5	29.3±0.3

Abbreviations: ε: Elongation; HT: Heat treatment; ODS: Oxide dispersion-strengthened; SLM: Selective laser melting; UTS: Ultimate tensile strength; YS: Yield strength.

The results of the microhardness measurements supported the conclusions regarding the quenched state of the material after SLM. The sample produced without pre-heating exhibited a value of microhardness of 441 ± 23 HV. The application of pre-heating was found to result in a reduction of material internal stresses by decreasing the thermal gradient, thereby leading to a decrease in microhardness to 390 ± 20 HV. After heat treatment, a microhardness of 288 ± 26 HV was measured.

These results underscore the need for a change in the heat treatment mode after SLM. The selected heat treatment mode was found to exert a negative impact on the tensile properties of the material. The results of the study indicated the formation of a quenched structure in as-built material and subsequent quenching within the heat treatment did not have a positive effect on the structure. Despite the lower values of average grain length and width, the specimens after heat treatment exhibited lower UTS values. During the heat treatment process, which involves quenching and high-temperature annealing, a recrystallization

phenomenon occurs, leading to the dissipation of internal stresses. This resulted in a reduction in tensile strength and an enhancement in ductility. In this instance, it is probable that the impact of grain size on strength properties is less significant than the impact of internal stresses. Therefore, we propose carrying out only high-temperature tempering for stress relief in future studies.

The presented results indicate the beneficial effects of the Y_2O_3 strengthening. Thus, the process of fabrication of ferritic/martensitic ODS steels through SLM should be further investigated. Further research is necessary to enhance the material's density and to conduct a thorough examination of its resulting microstructure. Further studies employing Transmission electron microscopy, Electron Backscatter Diffraction, and Small-angle X-ray scattering are necessary to investigate the size and distribution of the Y_2O_3. It is anticipated that in the future, this approach may facilitate the creation of material that exhibits both high strength and plastic properties.

4. Conclusion

In the present work, the ferritic/martensitic ODS steel with 0.25 wt.% Y_2O_3 was fabricated by SLM. The main conclusions of the study are summarized as follows:

(i) High material density, with a relative value of more than 98%, was achieved by adopting *VED* in the range of 80 – 110 J/mm^3 and platform pre-heating. *VED* is identified as the most significant factor affecting relative density in this work

(ii) After heat treatment, partial recrystallization of grains was noted, as indicated by a shift in grain morphology from elongated to more equiaxed forms. In addition, the grain size decreased as a result of partial recrystallization. The impact of pre-heating on the process of structure formation was also observed, resulting in the formation of elongated and narrow grains

(iii) At room temperature, reinforcement with 0.25 wt.% Y_2O_3 resulted in UTS values (978 MPa) of as-built material close to those for the similar ferritic/martensitic ODS steel plates and tubes fabricated by traditional methods. The selected heat treatment mode led to a substantial decrease in strength properties (UTS = 697 MPa), whereas ductility was increased. However, the obtained material exhibited brittleness, indicating the necessity of employing a different heat treatment mode to ensure both enhanced strength and plastic properties.

Acknowledgments

None.

Funding

This work is supported by the Russian Science Foundation (No. 23-79-30004, https://rscf.ru/project/23-79-30004/).

Conflicts of interest

The authors declare no conflicts of interest.

Author contributions

Conceptualization: Vadim Sufiiarov
Data curation: Maria Zaitceva
Funding acquisition: Anatoliy Popovich
Investigation: Maria Zaitceva, Artem Borisov
Project administration: Vadim Sufiiarov
Resources: Anatoliy Popovich
Supervision: Vadim Sufiiarov
Writing – original draft: Maria Zaitceva
Writing – review & editing: Vadim Sufiiarov

Ethics approval and consent to participate

Not applicable.

Consent for publication

Not applicable.

Availability of data

The data presented in this study are available on request from the corresponding author.

References

1. Li A, Chen Q, Wang P, *et al*. Microstructure and properties of oxide-reinforced FeCrAl matrix alloy manufactured by selective laser melting. *Mater Today Commun*. 2024;39:109226.

   doi: 10.1016/j.mtcomm.2024.109226

2. Wang M, Sun H, Zou L, Zhang G, Li S, Zhou Z. Structural evolution of oxide dispersion strengthened austenitic powders during mechanical alloying and subsequent consolidation. *Powder Technol*. 2015;272:309-315.

   doi: 10.1016/j.powtec.2014.12.008

3. Little EA, Stow DA. Void-swelling in irons and ferritic steels: II. An experimental survey of materials irradiated in a fast reactor. *J Nucl Mater*. 1979;87(1):25-39.

   doi: 10.1016/0022-3115(79)90123-5

4. Shashanka R. Non-lubricated dry sliding wear behavior of spark plasma sintered nano-structured stainless steel. *J Mater Environ Sci*. 2019;10(8):767-777.

5. Walker JC, Berggreen KM, Jones AR, Sutcliffe CJ. Fabrication of Fe-Cr-Al oxide dispersion strengthened PM2000 alloy using selective laser melting. *Adv Eng Mater*.

2009;11(7):541-546.

doi: 10.1002/adem.200800407

6. Wilms MB, Rittinghaus SK, Goßling M, Gökce B. Additive manufacturing of oxide-dispersion strengthened alloys: Materials, synthesis and manufacturing. *Prog Mater Sci*. 2023;133:101049.

doi: 10.1016/j.pmatsci.2022.101049

7. Suryanarayana C. Mechanical alloying and milling. *Prog Mater Sci*. 2001;46(1-2):1-184.

doi: 10.1016/S0079-6425(99)00010-9

8. Ou Lahcen EM, Ángel Alcázar MM, Almeida CP. New high strength ODS Eurofer steel processed by mechanical alloying. *Mater Sci Eng A*. 2021;817:141288.

doi: 10.1016/j.msea.2021.141288

9. Noh S, Choi BK, Kang SH, Kim TK. Influence of mechanical alloying atmospheres on the microstructures and mechanical properties of 15Cr ODS steels. *Nucl Eng Technol*. 2014;46(6):857-862.

doi: 10.5516/NET.07.2013.096

10. Verma L, Dabhade VV. Synthesis of Fe-15Cr-2W oxide dispersion strengthened (ODS) steel powders by mechanical alloying. *Powder Technol*. 2023;425:118554.

doi: 10.1016/j.powtec.2023.118554

11. Oksiuta Z, Ozieblo A, Perkowski K, Osuchowski M, Lewandowska M. Influence of HIP pressure on tensile properties of a 14Cr ODS ferritic steel. *Fusion Eng Design*. 2014;89(2):137-141.

doi: 10.1016/j.fusengdes.2014.01.052

12. Deng L, Luo J ru, Tu J, *et al*. Achieving excellent mechanical properties of ODS steel by Y2O3 addition. *Mater Sci Eng A*. 2023;872:145008.

doi: 10.1016/j.msea.2023.145008

13. Shi W, Yu L, Liu C, *et al*. Evolution of Y2O3 precipitates in ODS-316 L steel during reactive-inspired ball-milling and spark plasma sintering processes. *Powder Technol*. 2022;398:117072.

doi: 10.1016/j.powtec.2021.117072

14. Macía E, García-Junceda A, Serrano M, Hong SJ, Campos M. Effect of mechanical alloying on the microstructural evolution of a ferritic ODS steel with (Y-Ti-Al-Zr) addition processed by Spark Plasma Sintering (SPS). *Nucl Eng Technol*. 2021;53(8):2582-2590.

doi: 10.1016/j.net.2021.02.002

15. Zhao M, Zhang P, Xu J, *et al*. Optimization of microstructure and tensile properties for a 13Cr-1W ODS steel prepared by mechanical alloying and spark plasma sintering using pre-alloyed powder. *Mater Character*. 2024;207:113581.

doi: 10.1016/j.matchar.2023.113581

16. Li XP, Kang CW, Huang H, Sercombe TB. The role of a low-energy-density re-scan in fabricating crack-free $Al8_5Ni_5Y6Co_2Fe_2$ bulk metallic glass composites via selective laser melting. *Mater Des*. 2014;63:407-411.

doi: 10.1016/j.matdes.2014.06.022

17. Vasquez E, Giroux PF, Lomello F, *et al*. Elaboration of oxide dispersion strengthened Fe-14Cr stainless steel by selective laser melting. *J Mater Process Technol*. 2019;267:403-413.

doi: 10.1016/j.jmatprotec.2018.12.034

18. Sagaradze VV, Kozlov KA, Kataeva NV. Oxide-dispersion strengthened radiation-resistant steels. *Phys Met Metallogr*. 2018;119(13):1350-1353.

doi: 10.1134/S0031918X18130112

19. Tanno T, Ohtsuka S, Yano Y, Kaito T, Tanaka K. Effects of manufacturing process on impact properties and microstructures of ODS steels. *J Nucl Mater*. 2014;455(1):480-485.

doi: 10.1016/j.jnucmat.2014.07.075

20. Gil E, Ordás N, García-Rosales C, Iturriza I. Microstructural characterization of ODS ferritic steels at different processing stages. *Fus Eng Des*. 2015;98-99:1973-1977.

doi: 10.1016/j.fusengdes.2015.06.010

21. Hsiung LL, Fluss MJ, Kimura A. Structure of oxide nanoparticles in Fe-16Cr MA/ODS ferritic steel. *Mater Lett*. 2010;64(16):1782-1785.

doi: 10.1016/j.matlet.2010.05.039

22. Amini R, Alijani F, Ghaffari M, Alizadeh M, Okyay AK. Formation of B19′, B2, and amorphous phases during mechano-synthesis of nanocrystalline NiTi intermetallics. *Powder Technol*. 2014;253:797-802.

doi: 10.1016/j.powtec.2013.12.029

23. Smith TM, Thompson AC, Gabb TP, Bowman CL, Kantzos CA. Efficient production of a high-performance dispersion strengthened, multi-principal element alloy. *Sci Rep*. 2020;10(1):9663.

doi: 10.1038/s41598-020-66436-5

24. Ozerskoi N, Volokitina E, Razumov N, Popovich A. Mechanical properties of ODS steel fabrication by mechanical alloying and sparking plasma sintering. *AIP Conf Proc*. 2024;3154(1):020029.

doi: 10.1063/5.0201304

25. Jia H, Zhou Z, Li S. A new strategy for additive manufacturing ODS steel using Y-containing gas atomized powder. *Mater Character*. 2022;187:111876.

doi: 10.1016/j.matchar.2022.111876

26. Cakmak O, Yeom H, Cho JW. *In-situ* synthesis of Yttria-based precipitates and their effects on Fe12Cr6Al in laser powder bed fusion. *J Mater Res Technol*. 2024;33:6714-6721.

doi: 10.1016/j.jmrt.2024.11.059

27. Autones L, Aubry P, Ribis J, Leguy H, Legris A, De Carlan Y. Assessment of ferritic ODS steels obtained by laser additive manufacturing. *Materials* (*Basel*). 2023;16(6):2397.

doi: 10.3390/ma16062397

28. Zhai W, Zhou W, Nai SML. Effect of interface wettability on additively manufactured metal matrix composites: A case study of 316L-Y2O3 oxide dispersion-strengthened steel. *Metals*. 2024;14(2):170.

doi: 10.3390/met14020170

29. Jia H, Sun H, Wang H, Wu Y, Wang H. Scanning strategy in selective laser melting (SLM): A review. *Int J Adv Manuf Technol*. 2021;113(9):2413-2435.

doi: 10.1007/s00170-021-06810-3

30. Polekhina NA, Litovchenko IY, Tyumentsev AN, Astafurova EG, Chernov VM, Leontyeva-Smirnova MV. The effect of tempering temperature on the features of phase transformations in the ferritic-martensitic steel EK-181. *J Nucl Mater*. 2014;455(1-3):496-499.

doi: 10.1016/j.jnucmat.2014.08.012

31. Qin SS. *Influence of Preheating Temperature on Microstructure Evolution and Hardness of High-Speed Steel AISI M50 Processed by Laser Powder Bed Fusion - Qin - 2023 - Steel Research International*. Wiley Online Library. https://onlinelibrary.wiley.com/doi/10.1002/srin.202200784 [Last accessed on 2025 Jan 29].

32. Qin S, Saewe J, Kunz J, *et al*. Influence of preheating temperature on microstructure evolution and hardness of high-speed steel AISI M50 processed by laser powder bed fusion. *Steel Res Int*. 2023;94(6):2200784.

doi: 10.1002/srin.202200784

33. Masuo H, Tanaka Y, Morokoshi S, *et al*. Effects of defects, surface roughness, and HIP on fatigue strength of Ti-6Al-4V manufactured by additive manufacturing. *Proc Struct Integr*. 2017;7:19-26.

doi: 10.1016/j.prostr.2017.11.055

34. Shi Y, Lu Z, Xu H, Xie R, Ren Y, Yang G. Microstructure characterization and mechanical properties of laser additive manufactured oxide dispersion strengthened Fe-9Cr alloy. *J Alloys Compd*. 2019;791:121-133.

doi: 10.1016/j.jallcom.2019.03.284

35. Spiridonova KV, Litovchenko IYu, Polekhina NA, *et al*. Structural-phase transformations of 12% chromium ferritic-martensitic steel EP-823. *Izv Ferrous Metall*. 2023;66(6):725-732.

doi: 10.17073/0368-0797-2023-6-725-732

36. Wang Z, Liu Z, Ma J, *et al*. Investigation on microstructure and mechanical properties of electron-beam-welded joint of reduced activation ferritic/martensitic steel fabricated by selective laser melting. *Mater Sci Eng A*. 2023;881:145333.

doi: 10.1016/j.msea.2023.145333

37. Seede R, Zhang B, Whitt A, *et al*. Effect of heat treatments on the microstructure and mechanical properties of an ultra-high strength martensitic steel fabricated via laser powder bed fusion additive manufacturing. *Addit Manuf*. 2021;47:102255.

doi: 10.1016/j.addma.2021.102255

38. Zaitceva M, Erutin D, Popovich A, Sufiiarov V. Effect of pre-heating during selective laser melting of chromium steel on structure and properties. *Global Energy*. 2024;30(3):43-51.

doi: 10.18721/JEST.30303

39. Ghayoor M, Mirzababaei S, Lee K, *et al*. Strengthening of 304L Stainless Steel by Addition of Yttrium Oxide and Grain Refinement during Selective Laser Melting. In: *Solid Freeform Fabrication 2019: Proceedings of the 30th Annual International Solid Freeform Fabrication Symposium-An Additive Manufacturing Conference*; 2019. p. 967-976.

40. Sagaradze VV, Kochetkova TN, Kataeva NV, *et al*. Structure and creep of Russian reactor steels with a BCC structure. *Phys Metals Metallogr*. 2017;118(5):494-506.

doi: 10.1134/S0031918X17050131

41. Votinin SN, Balashov VD, Krylov EA, *et al*. Effect of Neutron Irradiation on High-Temperature Properties of Stainless Steels type Cr13 (Влияние Нейтронного Облучения на Высокотемпературные Свойства Нержавеющих Сталей Типа Х13). In: *Proceedings of the Scientific and Technical Conference "Nuclear Energy: Fuel Cycles, Radiation Materials Science", Ulyanovsk, October 5-10*; 1971. p. 351-379.